A non-classical crystallization mechanism of microbially-induced disordered dolomite

Deng Liu, Ting Chen, Zhaoyi Dai, Dominic Papineau, Xuan Qiu, Hongmei Wang, Karim Benzerara

A non-classical crystallization mechanism of microbially-induced disordered dolomite

Deng Liu[1, 2, *], Ting Chen[1], Zhaoyi Dai[1], Dominic Papineau[1, 3], Xuan Qiu[1], Hongmei Wang[1, 2], and Karim Benzerara[4]

[1]State Key Laboratory of Biogeology and Environmental Geology, China University of Geosciences, Wuhan 430078, China

[2]School of Environmental Studies, China University of Geosciences, Wuhan 430078, China

[3]Department of Earth Sciences, London Centre for Nanotechnology, and Center for Planetary Sciences, University College London, 17-19 Gordon Street, London, UK

[4]Sorbonne Université, Muséum National d'Histoire Naturelle, UMR CNRS 7590, Institut de Minéralogie, de Physique des Matériaux et de Cosmochimie (IMPMC), 4 Place Jussieu, 75005 Paris, France

Corresponding author: Deng Liu (liudeng@cug.edu.cn)

Revised for *Geochimica et Cosmochimica Acta*

April 30, 2024

ABSTRACT

Non-classical crystallization pathways, involving the formation of complex precursors prior to nucleation, have been observed during the calcification process of invertebrate skeletons and shells. However, these pathways were rarely documented in microbially-induced carbonate precipitation. In this study, we presented experimental evidence demonstrating that a halophilic bacterium (*Halomonas* sp. strain JBHLT-1) catalyzed the biomineralization of disordered dolomite through an amorphous calcium-magnesium carbonate (ACMC) with a stoichiometry near that of dolomite. During the ACMC formation, strain JBHLT-1 significantly enhanced the incorporation of Mg^{2+} ions compared to abiotic ACMC that was synthesized without any microbial biomass. In the stage of ACMC crystallization, the presence of microbial biomass reduced the dissolution-reprecipitation rate and induced bias towards a solid-state reaction pathway. This observation was supported by the negligible loss of structural Mg^{2+} ions in the presence of cells of strain JBHLT-1. The microbially-induced growth of disordered dolomite appeared to follow a spherulitic growth mechanism, as evidenced by its hierarchical structure composed of coalesced nano-spheres, eventually growing into micron-sized spheroids and dumbbells with extended incubation times. Since disordered dolomite is considered as a crucial crystalline precursor of ordered sedimentary dolomite, the findings of this study have important implications for understanding the formation mechanism of natural dolomite.

Keywords: microbial dolomite formation, dolomite problem, disordered dolomite, amorphous precursor, non-classical crystallization

1. Introduction

Crystallization is a ubiquitous natural phenomenon that creates an array of solid compounds, such as minerals and bio-macromolecules. The process of crystallization involves two critical steps: nucleation and growth. According to the classical crystallization theory (CCT), nucleation occurs through the direct addition of monomeric units, such as ions, atoms, or molecular species, and the subsequent growth process follows the terrace-ledge-kink mechanism (Mullin, 2001). The CCT model has been widely used to interpret the thermodynamics of crystal formation in geological, biological, and synthetic systems.

In spite of the successful application of CCT in a wide range of precipitation systems, this theory fails to explain certain unexpected phenomena in both nucleation and crystal growth (De Yoreo et al., 2009, 2015; Rodriguez-Blanco et al., 2011; Jehannin et al., 2019; Du et al., 2024). For instance, growing evidence shows that amorphous calcium carbonate (ACC) is often observed during the pre-nucleation stages of $CaCO_3$ polymorph crystallization, such as calcite, aragonite, and vaterite (e.g., Rodriguez-Blanco et al., 2011; Rodriguez-Navarro et al., 2015; Purgstaller et al., 2016). Furthermore, some other amorphous phases (e.g., amorphous calcium phosphate) are found to be vital precursors to their related crystalline forms in minerals (e.g., Lotsari et al., 2018). Not limited to amorphous particles, other complex species including clusters, oligomers or droplets can also function as nucleation precursors instead of simple atomic/molecular monomers postulated by CCT (De Yoreo et al., 2009, 2015). These nucleation pathways involve complex precursors at the pre-nucleation stage and differ significantly from the monomer-by-monomer addition process. In addition, crystals can also grow nonclassically by aggregation of nanoparticles (De Yoreo et al., 2015). As such, the term "non-classical crystallization" (NCC) has been used to describe these non-traditional pathways (De Yoreo et al., 2015; Jehannin et al., 2019). Growing experimental evidence showed that NCC is a common route to the formation of carbonate shells and skeletons in invertebrates, as evidenced by the presence of transient ACC (Addadi et al., 2003; Gong et al., 2012; Grünewald et al., 2022). However, it remains unclear whether the NCC model can correctly explain microbially-mediated carbonate precipitation, a common crystallization phenomenon observed in natural settings (Dong et al., 2022), although some cyanobacteria have been tentatively shown to produce intracellular ACC (Benzerara et al., 2014; Mehta et al., 2023).

Dolomite [$CaMg(CO_3)_2$] is one of the widely studied carbonate minerals, mainly due to the long-standing debate about the formation mechanism of sedimentary dolomite, an outstanding enigma of Earth sciences that is frequently called "dolomite problem" (Arvidson and Mackenzie, 1999; Gregg et al., 2015). The "dolomite problem" originates from the uneven distribution of dolomite abundance in the geological records and the experimental difficulties to precipitate ordered dolomite at ambient temperature (Warren et al., 2000; McKenzie and Vasconcelos, 2009; Xu et al., 2013). A huge amount of research has been conducted to unravel the mechanisms and kinetics of dolomite crystallization, and one of most exciting achievements is that microbial activity can overcome the kinetic barriers to dolomite nucleation (e.g., Vasconcelos et al., 1995; Roberts et al., 2004; Sánchez-Román et al., 2008; McKenzie and Vasconcelos, 2009; Deng et al., 2010; Bontognali et al., 2014; Petrash et al., 2017; Liu et al., 2019a, 2020a, 2020b; Han et al., 2022, 2024). It has been thought that microorganisms catalyze the formation of low-temperature of dolomite by increasing the dehydration rate of Mg^{2+} (Kenward et al., 2013). Since microbially-induced dolomites produced in most experimental studies are Mg-Ca disordered (Gregg et al., 2015), they should be termed as disordered dolomite or protodolomite *stricto senso*

(Zhang et al., 2012; Gregg et al., 2015; Kaczmarek et al., 2017). Disordered dolomite (with 36-55 mol% Mg^{2+}) possesses the same space group as calcite, but with a higher Mg content compared with Mg-calcite (<36 mol% Mg^{2+}) (Zhang et al., 2012). Nevertheless, given the metastable nature of disordered dolomite, it can progressively transform into ordered dolomite under burial conditions (Zheng et al., 2021). In this regard, the contribution of microbes to the genesis of sedimentary dolomite should be not neglected.

Noticeably, recent abiotic synthesis experiments have highlighted the potential involvement of the NCC pathway in the precipitation of Ca-Mg carbonates, particularly under high saturation conditions. For example, Al Disi et al. (2021) suggested that the formation of high-Mg calcite and other Mg-rich carbonates proceeds through Mg-bearing amorphous intermediates, which also potentially contribute to the genesis of disordered dolomite. While microbes are widely acknowledged as facilitators in the crystallization of low-temperature disordered dolomite, direct evidence supporting the application of the NCC theory for the formation of biotic disordered dolomite remains elusive. Specifically, two questions need to be addressed: (i) what is the amorphous phase that acts a prerequisite to the nucleation of disordered dolomite? and (ii) how do microbes govern the phase evolution? To shed light on these issues, we conducted cultivation experiments using *Halomonas* sp. strain JBHLT-1, a halophilic bacterium known to mediate the formation of disordered dolomite, and investigated the crystallization behavior of microbially-induced disordered dolomite.

2. Materials and methods

2.1. Bacterial strain and culture medium

In previous studies, we have demonstrated the capability of several *Halomonas* species isolated from an Inner Mongolian saline lake called Lake Jibuhulangtu Nuur, China, to induce the formation of low-temperature disordered dolomite (Liu et al., 2019a; Zheng et al., 2021). Among these species, strain JBHLT-1 has exhibited the production of exceptionally pure disordered dolomite during cell growth (Liu et al., 2019a), making it an ideal model strain for investigating the crystallization process of microbially-induced disordered dolomite. Cells of *Halomonas* sp. JBHLT-1 were aerobically grown in a Luria-Bertani (LB) medium (pH=7.8) supplemented with 52.6 g/L NaCl. The incubation was conducted in the dark at 30 °C with gentle rotary shaking (160 rpm).

2.2. Experimental design

To gain a better understanding of the complex process involved in the formation of microbially-induced disordered dolomite, a series of experiments were conducted (Fig. 1). The objective of the first experiment was to detect any presence of an amorphous precursor phase associated with microbially-induced disordered dolomite. In the second experiment, the focus was on identifying the specific properties of the precursor phase. Lastly, the third experiment aimed to investigate the transformation process of amorphous phase into disordered dolomite in the presence of microbes.

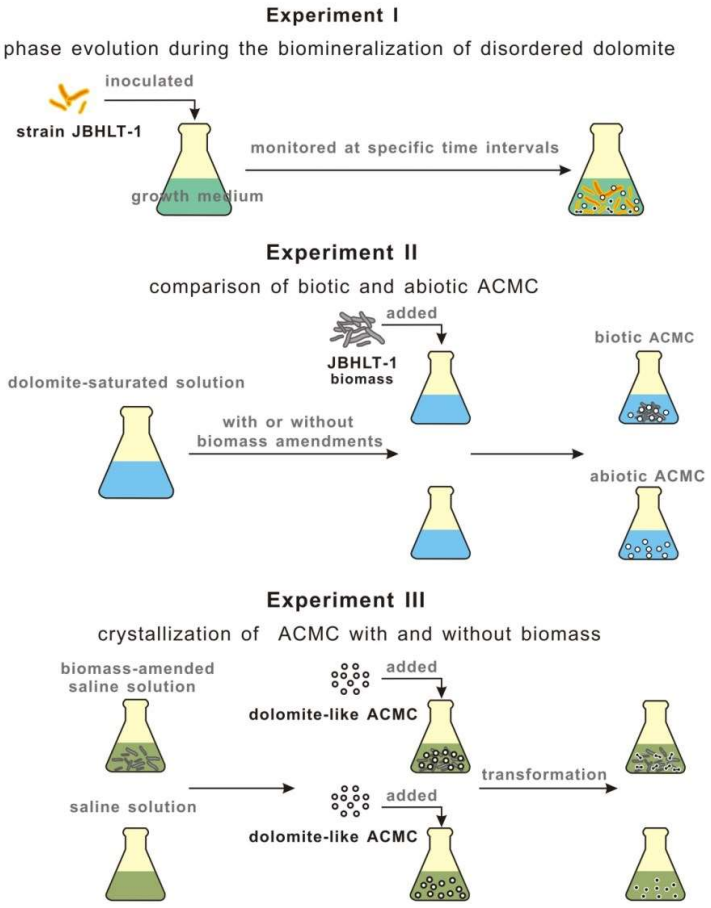

Fig. 1. Schematic detailing the experimental setup. The study consisted of three sets of experiments: Experiment I aimed to examine the potential amorphous precursor in the formation process of microbially-induced disordered dolomite; Experiment II compared the differences between biotic and abiotic ACMC; and Experiment III investigated the role of microbes in the ACMC transformation.

2.2.1. Experiment I: monitoring the crystallinity evolution of biotic disordered dolomite

Once the cells of strain JBHLT-1 reached the exponential growth phase, they were transferred to a precipitation medium with an initial OD_{600} of 0.1. The

precipitation medium consisted of the following components per liter: 511.1 mmol of NaCl, 50.0 mmol of $MgCl_2$, 10.0 mmol of $CaCl_2$, 117.5 mmol of Na_2SO_4, 0.5 mmol of $NaHCO_3$, 0.4 mmol of Na_2CO_3, 0.8 mmol of KCl, 0.5 g of bacto peptone, and 2 g of yeast extract (Liu et al., 2019a). The ion concentrations in this medium were chosen to mimic surface water chemistry of Lake Jibuhulangtu Nuur (Liu et al., 2019a). The pH of the medium was adjusted to 7.8 using 0.2 M NaOH. To ensure sterility without inducing precipitation, membrane filtration with a pore size of 0.22 μm (millipore, USA) was employed for sterilizing the medium instead of thermal autoclaving. The abiotic controls were identical to the biotic systems, except that cells were replaced with an equal volume of medium. All experimental flasks, including both biotic and abiotic systems, were incubated in the dark at 30 °C and shaken at 160 rpm in duplicate. During the bioprecipitation process of disordered dolomite, the solid products and solution compositions were monitored at specific time intervals. This allowed the assessment of any precursor phase involved in the crystallization of disordered dolomite.

2.2.2. Experiment II: comparative characterization of biotic vs. abiotic amorphous calcium-magnesium carbonate (ACMC)

In our biomineralization experiments, a precursor phase known as ACMC was observed prior to the formation of disordered dolomite (please refer to Section 3.2 for details). Interestingly, the ACMC is not exclusive to biologically-mediated processes but has also been commonly detected in abiotically synthetic experiments involving Ca-Mg carbonates (e.g., Rodriguez-Blanco et al., 2015). To explore the differences between biotic ACMC and its abiotic counterpart, additional synthesis experiments were carried out.

The biotic and abiotic ACMC were synthesized by direct precipitation in an aqueous solution containing 50.0 mM $MgCl_2$, 10.0 mM $CaCl_2$, and 60.0 mM Na_2CO_3, with or without the wet biomass of strain JBHLT-1. The biomass concentration used was 0, 0.25, and 0.50 g/L. The concentrations of Mg^{2+} and Ca^{2+} were identical to those used in the aforementioned bioprecipitation experiment. The concentration of HCO_3^- was set at a similar level determined in the bioprecipitation experiment when

ACMC was formed (see Section 3.2 for more details). Once white precipitates appeared, these suspensions were immediately separated by centrifugation (10000×g, 10 min). To prevent the crystallization of precursor phases in the water, the precipitates were rinsed in pure ethanol with gentle sonication and then freeze-dried using a lyophilizer (Martin Christ, Germany). Subsequently, these freeze-dried samples were stored under vacuum (2.7 kPa) until the mineralogical analyses were conducted.

It has been shown that the cell surface of microbes is responsible for the adsorption of Mg^{2+} and Ca^{2+} ions, thereby initiating the formation of calcium-magnesium carbonates (e.g., Kenward et al., 2013; Qiu et al., 2017). The surface charge of strain JBHLT-1 was analyzed using a Malvern zetasizer (Nano ZS, Malvern Instruments, UK) at a pH range of 7 to 9. To investigate the specific functional groups responsible for cation adsorption on the cell surface, an adsorption experiment was conducted. 25 mg of wet biomass from strain JBHLT-1 was introduced into a 50 mL centrifuge tube containing a solution composed of 50 mM $MgCl_2$ and 10 mM $CaCl_2$. The tube was then agitated at 30 °C and 160 rpm for 6 hours. Subsequently, the biomass was recovered through freeze-drying. The pristine biomass and the adsorbed biomass were examined using X-ray photoelectron spectroscopy (XPS; ESCALAB 250Xi, Thermo Fisher, USA).

2.2.3. Experiment III: assessing the role of microbes in the crystallization of ACMC into disordered dolomite

According to Experiment II, it was found that biogenic ACMC induced by strain JBHLT-1 exhibited a stoichiometry similar to dolomite, while abiotic ACMC synthesized under the same conditions had significantly lower Mg content (more details can be found in Section 3.3). It is interesting to note that the synthesis of abiotic ACMC with near-dolomite stoichiometry (i.e., dolomite-like ACMC) can be achieved in the solutions with very high saturation state for dolomite (e.g., Purgstaller et al., 2021), a scenario that is rarely found in sedimentary settings. To gain insight into the specific role of microbes in the transformation process from ACMC to disordered dolomite, we performed further crystallization experiments using abiotic

dolomite-like ACMC as the starting material.

In these experiments, abiotic dolomite-like ACMC was synthesized following the reported protocol by Purgstaller et al. (2021). In brief, 50 mL of 0.5 M $CaCl_2$ was added into 50 mL of 1 M $MgCl_2$ solution with vigorous stirring. The resulting Ca-Mg solution was rapidly mixed with an equal volume of 0.5 M Na_2CO_3, leading to the formation of ACMC. This dolomite-like ACMC was collected and freeze-dried. For the crystallization experiments, 0.1 g of dolomite-like ACMC was introduced in a solution of $MgCl_2/CaCl_2$ (20 mL, 50 mM Mg^{2+} and 10 mM Ca^{2+}). The solution was either supplemented with JBHLT-1 biomass (0.5 g/L) or left unamended. The reactors were placed at 30 °C and stirred for 24 h.

2.3. Chemical analyses and mineral characterization

The cell density in the bioprecipitation systems was monitored by OD_{600}, using a UV-vis spectrophotometer (Shimadzu UV-1800, Japan). The supernatant pH was measured using a pH meter (Denver, USA). The alkalinity of the solution was determined by the methods described previously (Blondeau et al., 2018). The cations (Mg^{2+} and Ca^{2+}) were quantified with an inductively coupled plasma-optical emission spectrometry (ICP-OES; Thermofisher ICAP6300, USA). The above measurements were performed in duplicate. The concentrations of HCO_3^- and CO_3^{2-} in the medium were calculated based on the measured pH and alkalinity, using the Visual MINTEQ 3.1 program. On the basis of these data, the saturation index (SI) with respect to (disordered-) dolomite was calculated using the formula $SI = \log(IAP/K_{SP})$, where IAP denotes the ion activity product of carbonate minerals and K_{SP} is the solubility product of the corresponding minerals ($10^{-16.52}$ and $10^{-17.1}$ for disordered dolomite and ordered-dolomite, respectively; Zhang et al., 2021).

Multiple mineralogical techniques were employed to characterize the solid phases, including X-ray diffraction (XRD), Raman spectroscopy, atomic force microscopy (AFM), and scanning and transmission electron microscopy (SEM and TEM), and thermogravimetric analysis-coupled gas chromatography mass spectrometry (TGA-GC/MS). To prevent the conversion of ACMC into crystalline phases due to moisture exposure, the analyses were completed promptly after being removed from the vacuum. XRD measurements were carried out using a Bruker D8

Advance diffractometer, scanning from 5 to 55° 2θ with a step size of 0.02° per second. The XRD patterns were analyzed using the MDI JADE 6.0 system. The stoichiometry of disordered dolomite was determined by calculating the position of the (104) peak using a calibrated curve developed by Bischoff et al. (1983). The chemical composition of ACMC was determined by ICP-OES after digestion with 10% HNO_3 (trace metal grade). Raman spectra were recorded using a Renishaw RM-1000 spectrometer with a 514 nm laser, covering the range of 100-2000 cm^{-1}. AFM topographical imaging was conducted using a Bruker Multimode AFM system in contact mode at ambient conditions. The AFM probe utilized a standard Si_3N_4 microlever with free resonance frequencies around 200 kHz. The images were captured at a scan rate of 0.5-2 Hz. SEM samples were coated with Pt and imaged using a Hitachi SU8010 SEM (Hitachi, Japan) with energy-dispersive X-ray spectroscopy (EDS, Oxford Instruments, UK). The electron accelerating voltages for imaging and EDS analyses were 5 and 15 kV, respectively. The TEM observations were carried out using a JEOL 2100F TEM (JEOL, Japan) operating at 200 kV. The chemical compositions of the solid products were semi-quantitatively analyzed using an EDS system (Quantax 200, Bruker, Germany) in the scanning TEM (STEM) mode. Additionally, selected area electron diffraction (SAED) patterns were obtained to identify the mineral phases and evaluate their crystallinity. Prior to TEM analyses, samples were dispersed in pure ethanol and deposited on formvar-coated Cu grids. TGA-GC/MS measurements were conducted using a TGA-2050 analyzer (TA Instruments, USA). The samples were heated from room temperature to 1000 °C at a rate of 10 °C min^{-1} under N_2 atmosphere. GC/MS (Clarus 500, PerkinElmer, USA) was used to detect the CO_2 gas released during sample decomposition.

3. Results

3.1. Experiment I

3.1.1. Changes of aqueous chemistry during bioprecipitation of disordered dolomite

According to the OD_{600} values, substantial cell growth was observed in the bioreactors (Fig. 2a). By contrast, no OD_{600} change was evidenced in the abiotic sets. In the biotic sets, the OD_{600} values rapidly increased from 0.101 to 0.845 within the first 10 days, followed by a gradual decline to 0.553 at the end of the 30-day

incubation period. The growth of strain JHBH-1 resulted in the increase of pH (Fig. 2a) and alkalinity (Fig. 2b). Specifically, in the biotic sets, the pH increased from an initial value of ca. 7.78 to 8.40 at day 30, and the solution alkalinity increased from 3.904 (at day 0) to 150.038 mM by day 30. Conversely, these parameters remained relatively constant in the abiotic sets. As a consequence of microbial activity, the concentrations of Ca^{2+} and Mg^{2+} decreased gradually over time (Fig. 2c), indicating the occurrence of bioprecipitation of Ca-Mg carbonate(s) in the biosystems. Importantly, the concentrations of Ca^{2+} and Mg^{2+} decreased in a nearly 1:1 molar ratio. The calculated saturation indices revealed that both disordered and ordered dolomites in the biosystems were saturated during incubation (Fig. 2d).

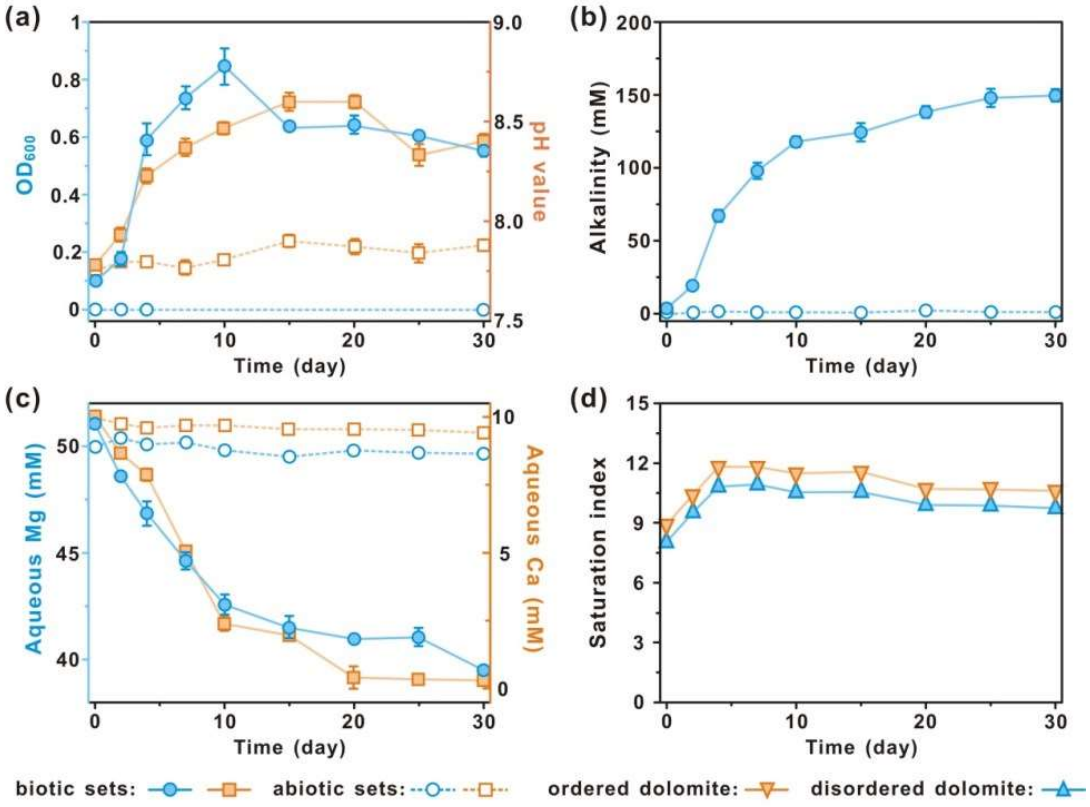

Fig. 2. Changes in wet chemistry parameters during the bioprecipitation of disordered dolomite by strain JBHLT-1: (a) OD600 and solution pH; (b) solution alkalinity; (c) concentrations of Mg^{2+} and Ca^{2+}; (d) SI for (disordered-)dolomite.

3.1.2. XRD, Raman and microscopic evidence for precursor ACMC involved in bioprecipitated disordered dolomite

After 4-day incubation, a visible cloudy precipitation was observed in the biosystems. The XRD data indicated that the solid phase at this stage was amorphous in nature, as indicated by the absence of distinct diffraction peaks. Instead, two broad humps were observed at 31.50° and 45.20° 2θ (Fig. 3a). Further, Raman analyses showed only one broad band at 1089 cm^{-1} over a noisy background (Fig. 3b). This band can be assigned to the internal vibration (v1) of CO_3^{2-}, confirming that this amorphous sample is a carbonate phase. Following 10-day incubation, several peaks

emerged in the XRD pattern (Fig. 3a). Notably, the characteristic peak at 30.76° 2θ (corresponding to a *d*-spacing of 2.904 Å) closely matched the (104) reflection of (disordered-)dolomite (Gregg et al., 2015). In addition, Raman analysis also revealed the presence of four distinct bands (Fig. 3b), which were consistent with those observed in disordered dolomite described in the literature (Fan et al., 2023). After extending the incubation period to 30 days, there was a noticeable improvement in the crystallinity of the precipitates, indicated by sharper and more intense XRD peaks (Fig. 3a). Such improvement was further supported by the presence of strong and well-defined Raman bands (Fig. 3b). However, it should be noted that even after the 30-day incubation period, the sample still lacked superlattice XRD peaks, such as (101), (015), and (021), suggesting that the final solid product induced by strain JBHLT-1 was disordered dolomite.

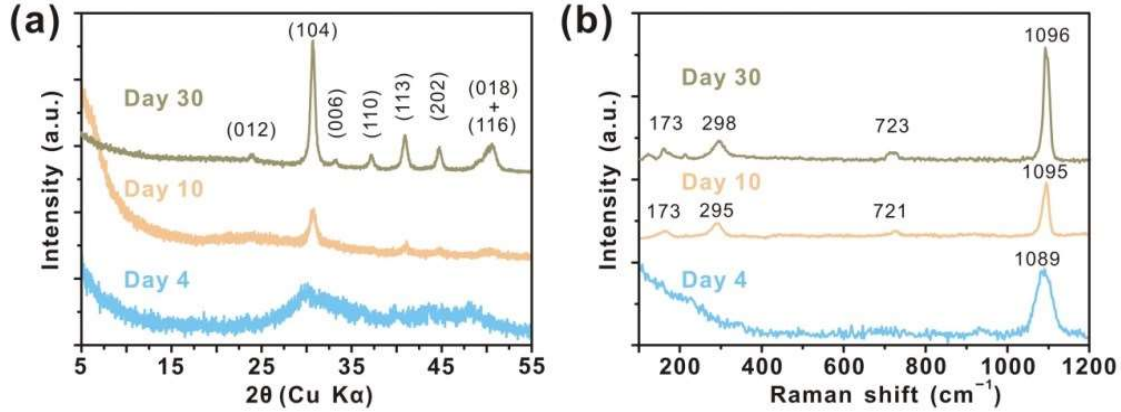

Fig. 3. XRD patterns with Miller indices (a) and Raman spectra (b) of bio-precipitates obtained at different time intervals.

The SEM images revealed that the amorphous solid phase collected on day 4 appeared as small clusters at the surface of cells or within microbial exopolysaccharides (EPS), forming irregular net-shaped structures (Fig. 4a). In STEM bright-field mode, the amorphous phase was observed as nano-spheres with an average size of 65 nm (Fig. 4b, c) and showed sensitivity to electron beam irradiation (Fig. 4c). The confirmation of its amorphous nature was shown by the presence of diffused halo rings in the SAED pattern (Fig. 4d). Semi-quantification of EDS analyses indicated that the amorphous phase had similar levels of Mg and Ca content (Fig. 4b), suggesting it could be identified as dolomite-like ACMC. After 10-day incubation, the bioprecipitates tended to coalesce into spheroids about 4 to 6 μm and with granular-texture surfaces (Fig. 4e). Despite this transformation, the chemical composition of these structures remained unaltered. The nano-subunits comprising these spheroids exhibited a mean size of 46 nm (Fig. 4e). Based on the EDS result and the earlier XRD data, these bioprecipitates were characterized as poorly-crystalline disordered dolomite. By day 30, the biogenic dolomite continued to grow in size, with the emergence of notable dumbbell-shaped morphologies around 20 μm in size (Fig. 4f). The surface of the dolomite dumbbells displayed clear cell imprints (Fig. 4f, inset), whereas AFM images revealed that the surface still consisted of nano-granular components (Fig. 4g). This observation was further supported by high-resolution

TEM (HRTEM) that showed a polycrystalline texture (Fig. 4h). Consistently, the corresponding SAED patterns clearly exhibited diffraction rings (Fig. 4h), supporting further its polycrystalline nature.

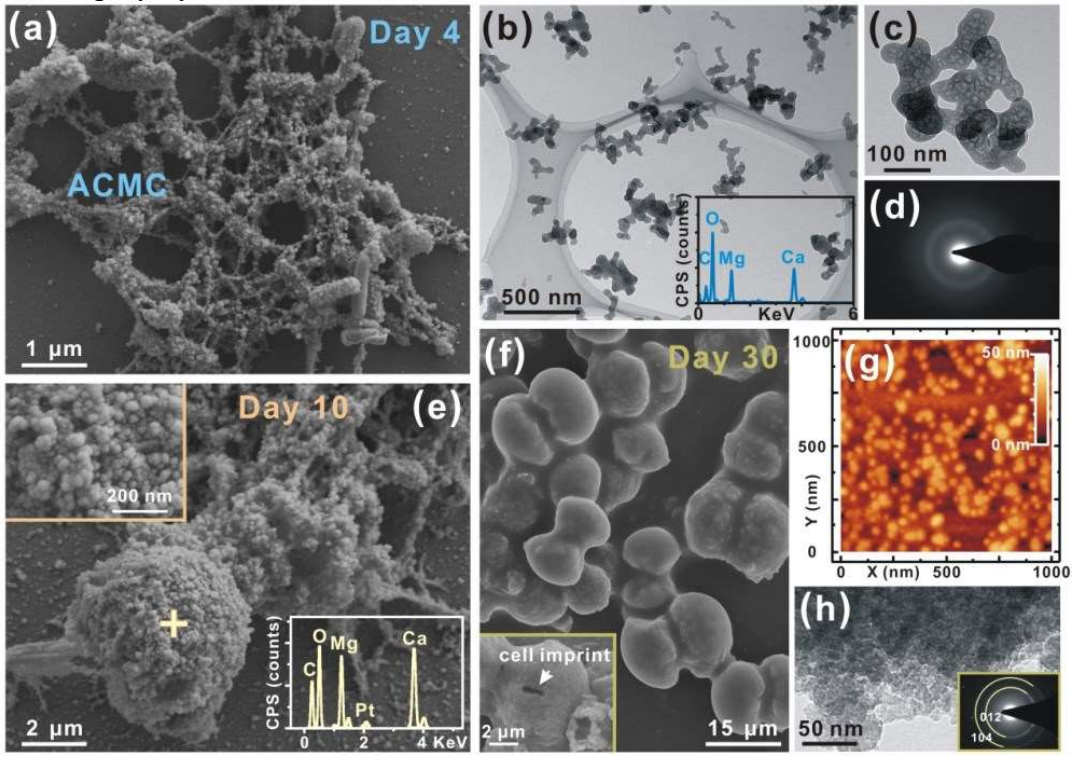

Fig. 4. Morphological changes of bio-precipitates during incubation: (a) SEM and (b-d) TEM-EDS-SAED images of the samples collected at day 4; (e) SEM-EDS results of the samples after 10-day incubation (the insert showing the granular-texture surfaces); (f-h) SEM, AFM and TEM images of the samples obtained at the end of experiments (the insert in panel f highlighting the cell imprints on the surface of disordered dolomite).

3.2. Experiment II

3.2.1. Comparison of biotic and abiotic ACMC

The XRD patterns of both biotic and abiotic ACMC showed a lack of crystalline peaks, confirming their amorphous nature (Fig. 5a). SEM results revealed that biogenic ACMC particles enclosed cells of stain JBHLT-1 (Fig. 5b), and this phenomenon became more pronounced with the presence of higher biomass (Fig. 5c). In contrast, the abiotic ACMC particles measured 75 nm on average, were found to be aggregated but not textured around cell-like morphologies (Fig. 5d).

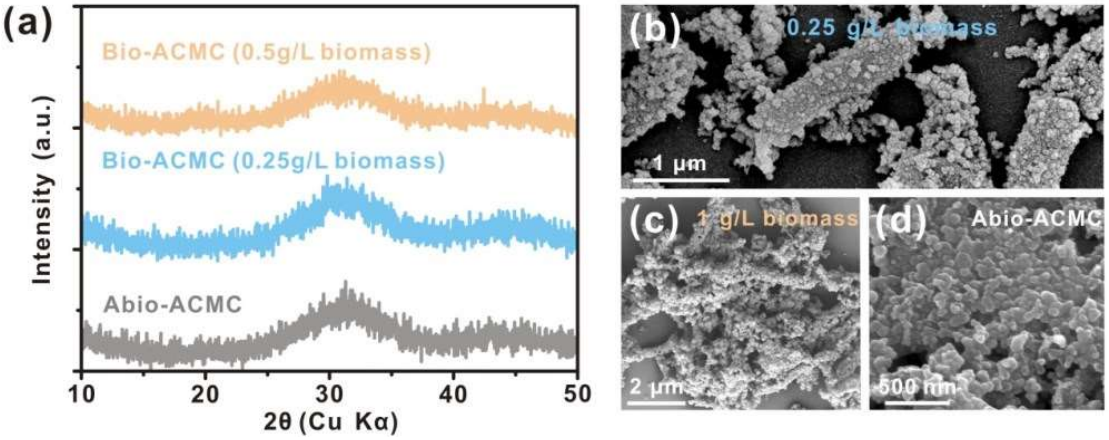

Fig. 5. Comparisons between abiotic and biotic ACMCs synthesized from same saturated solutions using XRD (a) and SEM (b).

The Mg contents of both biotic and abiotic ACMC were determined using TGA-GC/MS and ICP-OES (Fig. 6a-d). During the thermal decomposition process, both biotic and abiotic ACMC exhibited three distinct stages of weight loss. According to previous studies (e.g., Radha et al., 2012), the first stage below 320 °C was attributed to the dehydration of ACMC. The subsequent two stages, between 400-580 °C and 580-800 °C, were associated with the decarbonation processes of $MgCO_3$ and $CaCO_3$, respectively. Therefore, the relative intensities of the two CO_2 peaks generated during the thermal decomposition of ACMC can be used to determine the ratio of Mg to Ca present in this phase. As shown in Fig. 6a-c, the results showed that the intensity of the first CO_2 peak generated by $MgCO_3$ decomposition was the highest for biotic ACMC with 0.5 g/L biomass, followed by biotic ACMC with 0.25 g/L biomass and the abiotic counterpart. This indicates that the biomass of strain JBHLT-1 enhanced the loading of Mg^{2+} into ACMC. This observation was confirmed by ICP-OES, which showed that the Mg content of ACMC increased linearly with the dosage of biomass (Fig. 6d). It is interesting to note that the biotic ACMC sample with 0.5 g/L biomass had a $MgCO_3$ content of 48.77 mol%, qualifying it as dolomite-like ACMC.

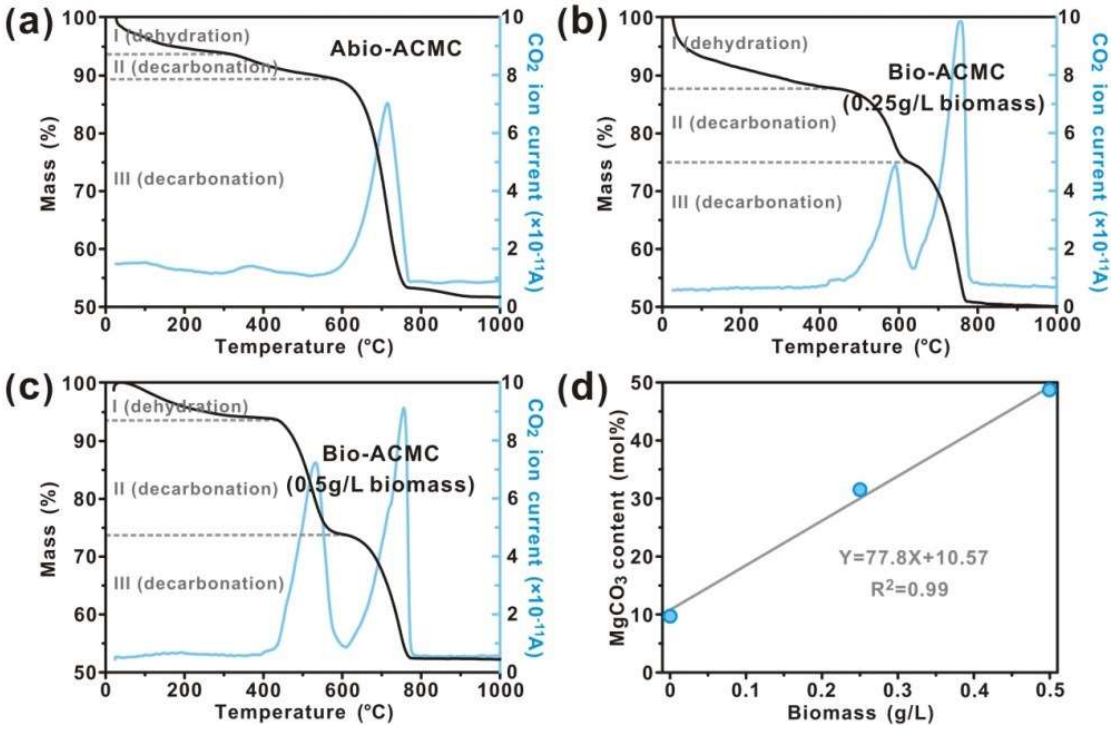

Fig. 6. (a-c) TGA-GC/MS profiles showing the differences of dehydration and decarbonation processes between abiotic and biotic ACMCs; (d) linear relationship between the biomass used and the Mg content of ACMC products.

3.2.2. Surface properties of strain JBHLT-1

The cell surface of strain JBHLT-1 was negatively-charged in the pH range of 7-9, as evidenced by the fact that the value of zeta potential was in the range of -55.2 to -63.8 mV (Fig. 7a). In addition, XPS spectra of the cell surface in the C 1s region

revealed three peaks at 284.7, 286.2, and 288 eV, which can be attributed to C-(C/H), C-OH, and O=C-O, respectively (Fig. 7b). The decrease in intensity of the peaks associated with O=C-O and C-OH after the adsorption of Mg^{2+}/Ca^{2+} indicated that these functional groups were involved in the cation adsorption process.

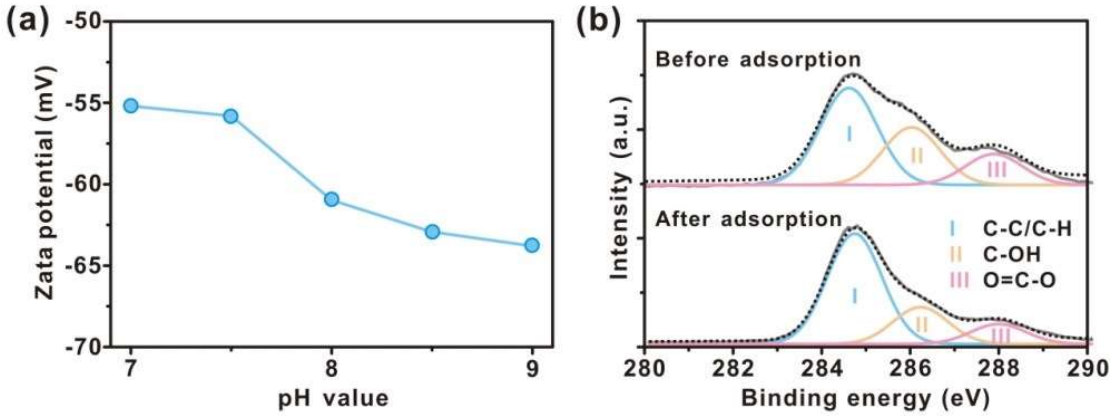

Fig. 7. (a) Zeta potential of cells of strain JBHLT-1 at different pHs; (b) XPS spectra of the cell surface in the C 1s region before and after Mg^{2+}/Ca^{2+} adsorption.

3.3. Experiment III

The abiotic dolomite-like ACMC used for the transformation experiments was synthesized and characterized using SEM and TEM-SAED methods (Fig. 8a, b). Similar to the other ACMC phases previously mentioned, the abiotic dolomite-like ACMC primarily appeared as spherulite-like aggregates with an average particle size of 80 nm. Furthermore, the amorphous nature of the material was confirmed by SAED data, and EDS analysis indicated a chemical composition closely resembling dolomite.

The particles immersed for 24 hours in a Mg^{2+}/Ca^{2+} solution with and without biomass showed distinct Bragg peaks instead of broad humps (Fig. 8c). In the biomass-free systems, the predominant crystalline phases were high-Mg calcite (ca. 18.03 mol% $MgCO_3$) along with minor amounts of aragonite (Fig. 8c). The high-Mg calcite phase appeared as spheroidal aggregates with a smooth surface (Fig. 8d). On the other hand, the biomass-amended systems primarily consisted of disordered dolomite (ca. 49.21 mol% $MgCO_3$) as the main constituent (Fig. 8c). Similar to the high-Mg calcite phase, the disordered dolomite phase also formed spheroidal to botryoidal aggregates (Fig. 8e). However, these aggregates had a high density of surface pores (Fig. 8e). Notably, the size of these pores matched the cell diameter of strain JBHLT-1, suggesting that the microbial cells acted as templates during the crystallization process. Furthermore, HRTEM data revealed that the disordered dolomite sample consisted of nano-grains that were randomly oriented, as evidenced

by the occurrence of polycrystalline SAED patterns (Fig. 8f).

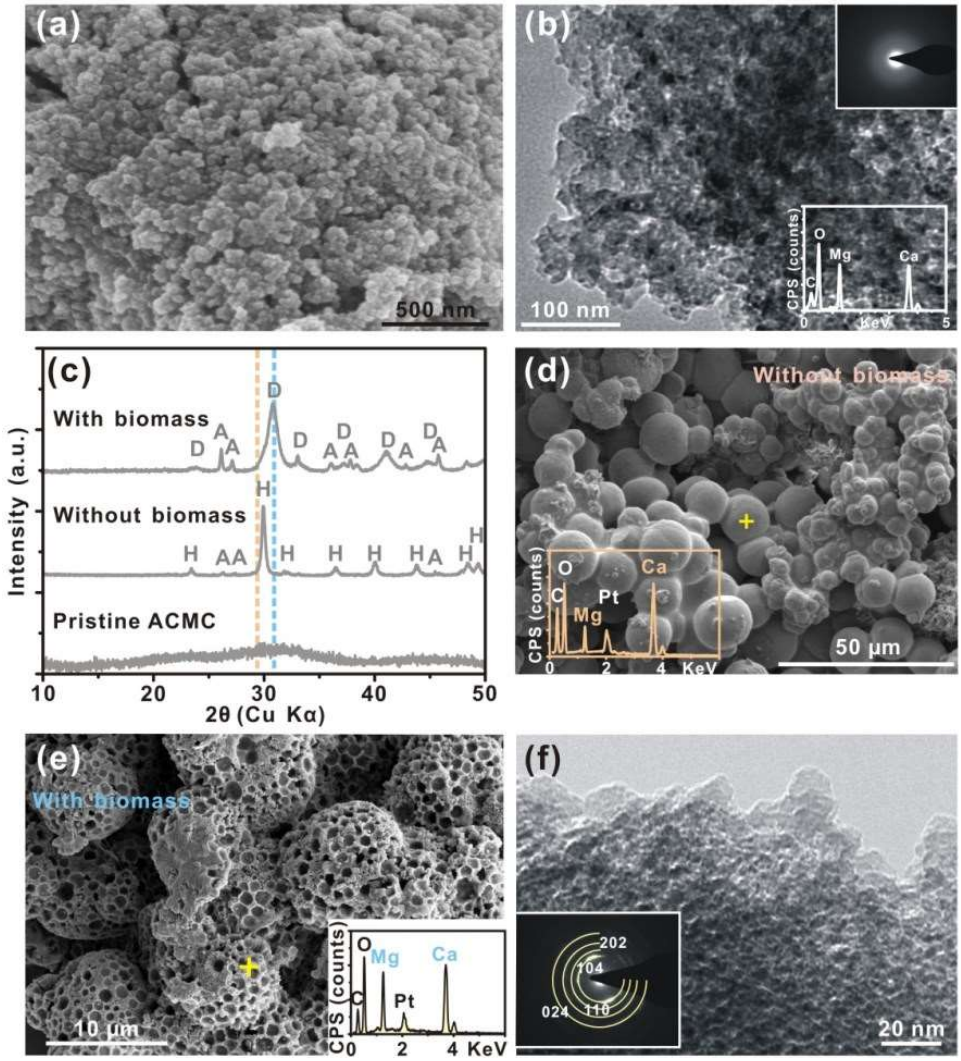

Fig. 8. The morphological and chemical features of abiotic dolomite-like ACMC (a-b) and comparisons the crystalline products after the transformation of abiotic ACMC in the absence and presence of the biomass of strain JBHLT-1 (c-f). (a) SEM data; (b) TEM data; (c) XRD patterns with the blue and orange lines respectively highlighting the (104) peak position of dolomite and calcite (D, disordered dolomite; A, aragonite; H, high-Mg calcite); (d) SEM-EDS data of high-Mg calcite obtained from the reactors without biomass; (e-f) SEM-EDS and TEM-SAED images of disordered dolomite collected from the reactors with biomass.

4. Discussion

4.1. The role of microbes in the formation of ACMC

In our biomineralization experiments (Experiment I) mediated by a halophilic bacterium, an amorphous phase was discovered preceding the nucleation of disordered dolomite. This phase was identified as Mg-bearing ACC (i.e., ACMC), based on the TEM-EDS-SAED data, supported by XRD and Raman analyses (Fig. 4). As previously noted, ACC has recently been recognized as a vital precursor of crystal

phases in the skeletal tissue and eggshells of animals. ACC is utilized by animals as a temporal storage site for calcium and carbonate ions, which are later employed in the rapid calcification process (Gong et al., 2012; Grünewald et al., 2022). ACC is also formed intracellularly by a diversity of bacteria, with a biological function that remains unknown (Monteil et al., 2021; Benzerara et al., 2022). It is also worth noting that ACC is commonly formed as a precursor of crystalline $CaCO_3$ (e.g., calcite, aragonite, and vaterite) in abiotic precipitation experiments under highly supersaturated forming solutions (e.g., Cam et al., 2015; Mergelsberg et al., 2020). In the context of our bioreactors, the saturation of carbonate minerals was significantly increased during the growth of strain JBHLT-1. For example, the SI reached as high as 10.90 for disordered dolomite and 11.48 for ordered dolomite (Fig. 2). This extensive supersaturation state was thus beneficial for the formation of ACC. Our previous study has demonstrated the capacity of strain JBHLT-1 to create supersaturated solutions with respect to crystalline carbonates (Liu et al., 2019a). In general, strain JBHLT-1 possesses the ability to increase solution pH through ammonification of peptone present in the precipitation medium (peptone → NH_3 + H_2O → NH_4^+ + OH^-) and elevate the solution alkalinity through respiration of yeast extract (yeast extract → CO_2 + H_2O → HCO_3^- + H^+) (Liu et al., 2019a). This was validated once again in our present study through measurements of solution pH and alkalinity under the action of stain JBHLT-1 (Fig. 2). In doing so, the high supersaturated condition created by strain JBHLT-1 allowed for the precipitation of ACMC from our precipitation medium, which contained sufficient amounts of Ca^{2+} and Mg^{2+} ions (Fig. 9).

Due to its highly hydrated and thermodynamically unstable nature, pure ACC tends to crystallize very rapidly in an aqueous solution. For instance, Rodriguez-Blanco et al. (2011) demonstrated that the complete breakdown of ACC occurred within 45 min at 7.5 °C and only 12 min at 25 °C. However, the addition of various substances, such as Mg^{2+} ions, can extend the lifetime of ACC (Ihli et al., 2013). Furthermore, it has been documented that the enhanced stability of ACC with elevated Mg content is due to the strong association between Mg^{2+} ions and structural water. This association effectively retards the dehydration process, a prerequisite step for crystallization (Purgstaller et al., 2016). In our biomineralization experiments, ACMC was observed to emerge at least by day 4 and persist until day 10 (Fig. 3). This long-lasting stability of our biogenic ACMC should be also attributed to its

421 remarkably high content of structural Mg^{2+}. The Mg content in this biogenic ACMC
422 was found to be the same as that of Ca (Fig. 4b), indicating a stoichiometry similar to
423 (disordered-)dolomite.
424 Given the high concentration of Mg (50 mM) in the precipitation medium, it is
425 not surprising that Mg^{2+} can be incorporated into the microbially-induced ACC. In
426 order to investigate the potential influence of microbes on the chemical composition
427 of ACMC, Experiment II was conducted. Both biotic and abiotic ACMC were
428 generated by mixing solutions of $CaCl_2$ (10 mM), $MgCl_2$ (50 mM), and Na_2CO_3 (60
429 mM), with the exception that biomass of strain JBHLT-1 was introduced to produce
430 biotic ACMC. Remarkably, the biotic ACMC exhibited significantly higher Mg
431 content compared with the abiotic counterpart. Moreover, the synthesis of
432 dolomite-like ACMC was achieved when 0.5 g/L biomass was used (Fig. 6d). These
433 findings suggest that the biomass of strain JBHLT-1 can accelerate Mg^{2+} uptake in
434 ACC. In fact, carboxyl-rich molecules have been shown to effectively load Mg^{2+} ions
435 into ACC, leading to the formation of ACMC (Wang et al., 2009). The positive role
436 of carboxyl-rich molecules arises from their capacity to bind Mg-H_2O complexes
437 through electrostatic attraction (Kenward et al., 2013; Liu et al., 2020b). This binding
438 results in the replacement of a water molecule in the Mg-H_2O complex by a carboxyl
439 group, leading to the generation of Mg-carboxyl clusters. Importantly, Mg-carboxyl
440 clusters require less energy for carbonation and subsequent attachment of Ca^{2+}
441 compared to Mg-H_2O complexes (Kenward et al., 2013; Roberts et al., 2013; Qiu et
442 al., 2017). As a consequence, the Mg content can be increased with the aid of
443 carboxyl-rich molecules. The surface of microbial cells is generally
444 negatively-charged (Fig. 7a) and contains a considerable concentration of functional
445 groups such as carboxylates (Fig. 9). These carboxyl groups mainly derive from the
446 surface-associated protein fractions. This characteristic was also observed in strain
447 JBHLT-1 (Fig. 7b). In addition to carboxyl groups, our XPS analysis indicated that
448 hydroxyl groups, likely associated with polysaccharides, are overlooked facilitators
449 for enhancing the signal of Mg^{2+} in ACMC (Fig. 7b). This finding supports the
450 emerging view that polysaccharides play a critical role in regulating the Mg content of
451 Ca-Mg carbonates (e.g., Al Disi et al., 2019).

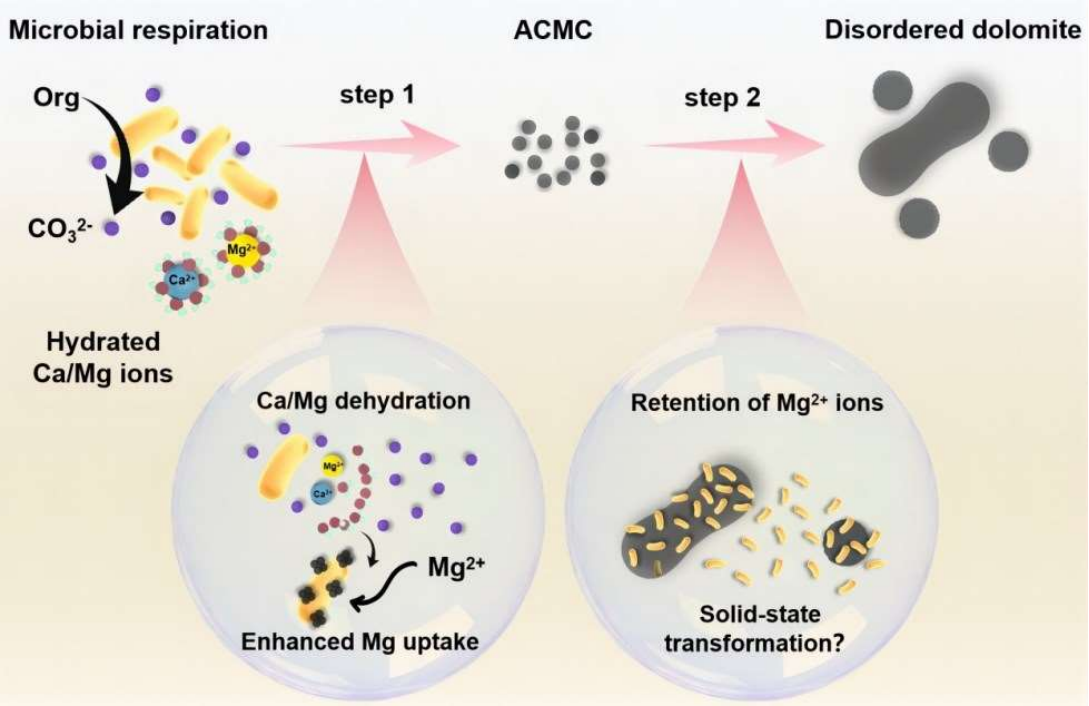

Fig. 9. Schematic diagram illustrating the interpreted role of microbes in the formation of disordered dolomite.

In addition to microbial cells, EPS might also be involved in the formation of ACMC obtained from our biomineralization experiments. Indeed, SEM observations showed that the ACMC nano-spheres were closely associated with both the cells of strain JBHLT-1 and EPS (Fig. 4a). Microbial EPS are known to be rich in various acid moieties, allowing them to serve as effective adsorbents for Mg^{2+} and Ca^{2+} (Zhang et al., 2015, 2021; Al Disi et al., 2019; Liu et al., 2020a). Therefore, EPS released by strain JBHLT-1 might potentially diminish the Mg-hydration effect in a manner similar to microbial biomass.

4.2. The effect of microbes on the transformation of ACMC

Previous studies have established that the ACC-type materials, including ACMC, exhibit a nanoporous framework structure (Purgstaller et al., 2016). This unique feature provides a large surface area that facilitates the exchange of solutes between ACMC and the surrounding reactive solution (Goetschl et al., 2021). While the incorporation of Mg^{2+} can act as a mitigating factor against the rapid crystallization of ACMC, it should be noted that when ACMC particles are exposed to bulk aqueous solutions, they tend to dissolve. In Experiment III, the transformation of abiotic ACMC occurred via a dissolution-reprecipitation route, resulting in the loss of Mg^{2+} from ACMC as attested by its transformation to high-Mg calcite with a Mg content lower than that of the initial ACMC. This finding is consistent with a recent study by Purgstaller et al. (2019), which demonstrated that ACMC containing ≥20 mol% Mg

472 released Mg^{2+} into solutions during its crystallization.

473 Interestingly, in the presence of 0.5 g/L biomass, disordered dolomite became the
474 primary product following ACMC transformation (Fig. 8c, f), suggesting that
475 microbial biomass has the potential to mitigate the Mg^{2+} loss from ACMC during the
476 crystallization process. Noticeably, the synthesis of Ca-Mg carbonates with high Mg
477 levels through ACMC transformation can be achieved by reducing the water activity.
478 Dry heating, for example, can induce the crystallization of ACMC into dolomite
479 through solid-state transformation (Sugawara et al., 2022). Furthermore, incorporating
480 Mg^{2+} into the Ca-Mg carbonates using ACMC as the precursor phase is also feasible
481 by lowering the water activity under mild solution conditions. For instance, Lenders
482 and his colleagues demonstrated that crystallization of ACMC in mixtures of organic
483 solvent (tetrahydrofuran or dioxane) and water can yield disordered dolomite
484 (Lenders et al., 2012). Similar observations have also been made in an aqueous
485 solution containing lipid vesicles (Yu et al., 2017). It has been proposed that the
486 adsorption of hydrophobic organic molecules onto the surface of ACMC creates a
487 hydrophobic layer (Yu et al., 2017). This layer limits the water content on the ACMC
488 surface, which in turn retards the dissolution-reprecipitation rate and favors the
489 solid-state reaction pathway, thereby retaining the Mg levels in Ca-Mg carbonates. A
490 similar mechanism may be involved in the ACMC transformation in the presence of
491 microbes. It has been well documented that microbes have both hydrophilic and
492 hydrophobic properties due to the presence of various functional groups on the
493 surface of cell wall and within EPS (van der Mei et al., 1998; Al Disi et al., 2019;
494 Zheng et al., 2021). Specifically, the hydrophobic nature of microbial cells is ascribed
495 to the presence of non-polar moieties, such as aromatics and aliphatic regions in
496 surface-associated proteins. In the case of strain JBHLT-1, our XPS data indicated a
497 high abundance of hydrophobic groups (C-C and C-H) and a lower abundance of
498 hydrophilic groups (C-OH and $O=C-O^-$) on the cell surface (Fig. 7b). Consequently,
499 when ACMC particles adhered to the cells of strain JBHLT-1, the cells could repel
500 some water molecules away from the particle surface using their non-polar moieties
501 and hydrophobic groups. In this regard, the conversion of ACMC to disordered
502 dolomite can be interpreted to most likely have occurred through a solid-state
503 transformation instead of the dissolution-reprecipitation process, explaining why in
504 this case the Mg content of the resulting crystalline byproduct remained high (Fig. 9).
505 The energy difference between ACMC and disordered dolomite should be the driving
506 force of this solid-state reaction.

4.3. The growth morphology of microbially-induced disordered dolomite

Based on our bioprecipitation experiments, it was observed that the poorly crystalline disordered dolomite at day 10 exhibited a polycrystalline microsphere structure, which was made of nanoparticulate subunits (Fig. 4e). Interestingly, the size of these nano-subunits was found to be smaller than that of ACMC. According to previous studies regarding ACC transformation, this change in size can be attributed to the dehydration of ACC and subsequent structural reorganization (Rodriguez-Blanco et al., 2011, 2015). At the end of the 30-day incubation, the size of biogenic disordered dolomite significantly increased, accompanied by a morphological change into a dumbbell shape (Fig. 4f). These dolomite dumbbells also consist of nano-sized subunits (Fig. 4g, f). These features strongly suggest that the growth of biogenic disordered dolomite occurred through a spherulitic mechanism (Gránásy et al., 2005; Rodriguez-Blanco et al., 2011). Spherulitic growth is known for its rapid process, where new nanoparticles continuously nucleate on the surface of pre-existing particles (Rodriguez-Blanco et al., 2011). To achieve such fast crystallization, high supersaturation (SI > 2~3) is necessary (Gránásy et al., 2005). Because solution saturation commonly acts as the thermodynamic driving force that not only governs the crystal growth rate but also impacts its shape (Gránásy et al., 2005). At moderate levels of supersaturation (i.e., insufficient driving force), crystals form in equilibrium with their morphology primarily determined by the shape of their unit cell. However, increasing the levels of supersaturation can lead to the formation of dendritic polycrystals with highly disequilibrium morphology, often appearing as spherular radial structures (Gránásy et al., 2005). In our specific bioprecipitation experiments, the microbial activity resulted in a high SI (> 8) for (disordered-)dolomite (Fig. 2d), which was maintained throughout the entire incubation period, thus promoting a high crystallization rate.

4.4. Geological implications

Through three sets of experiments, we demonstrated that microbially-induced disordered dolomite proceeded through spherulitic growth, with ACMC serving as a transient phase. As a consequence, microbially-induced disordered dolomite was made of numerous nanoparticles, consistent with previous studies (e.g., Bontognali et al., 2008; Liu et al., 2019a). Nanoparticle aggregates have been observed in Holocene dolomites (e.g., Bontognali et al., 2010; Nyirö-Kása et al., 2018; Raudsepp et al., 2022), as well as in some ancient dolomites (Perri and Tucker, 2007; Sánchez-Román et al., 2008; Sun et al., 2023). This unique morphology and texture were considered as potential biomarkers suggesting microbial activity or the presence of fossilized bacteria or viruses (e.g., Perri and Tucker, 2007; Sun et al., 2023). Our findings, along

with others, highlight that this NCC pathway requires strongly supersaturated solutions. It is relevant to note that similar spherulitic microscopic objects have been synthesized in abiotic disordered dolomite as well (Rodriguez-Blanco et al., 2015; Liu et al., 2019b). Therefore, this particular microscopic morphology is indicative of fluid chemistry conditions under which dolomite is formed and cannot serve as a biosignature. Apart from the specific morphology mentioned above, it has been documented that calcite formed via ACC has unique geochemical signatures compared to directly-precipitated calcite, such as higher trace element contents (Littlewood et al., 2017). However, future experiments are necessary to determine whether this phenomenon also applies to microbially-induced disordered dolomite.

In numerous biomineralization experiments, including our present study, microbial activity has consistently been observed to result in the formation of disordered dolomite, rather than its ordered counterpart. In contrast, in Holocene dolomite-forming environments, the dolomites found are frequently partially-ordered, such as calcian dolomite (Gregg et al., 2015; Petrash et al., 2017). It has been proposed that the gradual conversion of disordered dolomite to ordered dolomite can be initiated through a diagenesis-controlled recrystallization process. Previous modeling work showed that this ordering process is relatively slow, taking several decades and even longer at low temperatures (<40 °C) (Arvidson and Mackenzie, 1999). However, a recent study by Kim et al. (2023) provides new experimental and computational evidence that reveals that fluctuations in supersaturation can greatly expedite the ordering reaction. Therefore, even in very early diagenesis, if the surrounding fluids are dynamic and fluctuating, the alteration of disordered dolomite can progress towards ordered dolomite.

5. Conclusions

During the bioprecipitation process of disordered dolomite by *Halomonas* sp. JBHLT-1, an amorphous calcium-magnesium carbonate solid known as ACMC was identified as a crucial precursor. This biogenic ACMC exhibited spherical nanocrystals with a near-dolomite stoichiometry. The formation of dolomite-like ACMC was attributed to the activities of strain JBHLT-1. These activities included the creation of highly supersaturated conditions and the facilitation of Mg^{2+} loading into ACMC by diminishing the Mg-hydration effect through the strong capacity of microbial cells and EPS to bind Mg^{2+} ions. Strain JBHLT-1 played an important role in the crystallization of ACMC to disordered dolomite because the presence of microbial cells could reduce the Mg loss during the ACMC transformation. The resulting disordered dolomite appeared in the form of aggregates composed of

nanoscopic grains. These findings indicate that the formation of microbially-induced disordered dolomite follows a NCC pathway and exhibits spherulitic growth. Hence, spherulitic dolomite habits cannot be used alone to discriminate between abiotic and biotic dolomite.

CRediT authorship contribution statement

Deng Liu: Conceptualization, Data curation, Funding acquisition, Methodology, Writing-original draft. **Ting Chen:** Formal analysis, Investigation, Data curation. **Zhaoyi Dai:** Data curation. **Dominic Papineau:** Data curation. **Xuan Qiu:** Data curation. **Hongmei Wang:** Data curation. **Karim Benzerara:** Data curation, Writing-original draft.

Data availability

Data are available through Mendeley Data at https://10.17632/986xbx3hh7.1.

Acknowledgements

This project was funded by the National Natural Science Foundation of China (Nos. 42330201, 42272046 and 42202035) and the 111 Project (No. BP0820004).

References

Addadi, L., Raz, S., Weiner, S., 2003. Taking advantage of disorder: Amorphous calcium carbonate and its roles in biomineralization. Adv. Mater. 15(12), 959-970.

Al Disi, Z.A., Zouari, N., Dittrich, M., Jaoua, S., Al-Kuwari, H.A.S., Bontognali, T.R.R., 2019. Characterization of the extracellular polymeric substances (EPS) of Virgibacillus strains capable of mediating the formation of high Mg-calcite and protodolomite. Mar. Chem. 216, 103693.

Al Disi, Z.A., Zouari, N., Attia, E., Al-Asali, M., Al-Kuwari, H.A.S., Sadooni, F., Dittrich, M., Bontognali, T.R.R., 2021. Systematic laboratory approach to produce Mg-rich carbonates at low-temperature. RSC Adv. 11, 37029.

Arvidson, R.S., Mackenzie, F.T., 1999. The dolomite problem: control of precipitation kinetics by temperature and saturation state. Am. J. Sci. 299, 257-288.

Benzerara, K., Skouri-Panet, F., Li, J., Férard, C., Gugger, M., Laurent, T., Couradeau, E., Ragon, M., Cosmidis, J., Menguy, N., Margaret-Oliver, I., Tavera, R., López-García, P., Moreira, D., 2014. Intracellular Ca-carbonate biomineralization is widespread in cyanobacteria. Proc. Natl. Acad. Sci. U. S. A. 111(30), 10933-10938.

Benzerara, K., Duprat, E., Bitard-Feildel, T., Caumes, G., Cassier-Chauvat, C., Chauvat, F., Dezi, M., Diop, S.I., Gaschignard, G., Görgen, S., Gugger, M., López-García, P., Millet, M., Skouri-Panet, F., Moreira, D., Callebaut, I.,

2022. A new gene family diagnostic for intracellular biomineralization of amorphous Ca carbonates by cyanobacteria. Genome Biol. Evol. 14(3), evac026.

Bischoff, W.D., Bishop, F.C., Mackenzie, F.T., 1983. Biogenically produced magnesian calcite: inhomogeneities in chemical and physical properties; comparison with synthetic phases. Am. Mineral. 68, 1183-1188.

Blondeau, M., Sachse, M., Boulogne, C., Gillet, C., Guigner, J.M., Skouri-Panet, F., Pionsot, M., Ferard, C., Miot, J., Benzerara, K., 2018. Amorphous calcium carbonate granules form within an intracellular compartment in calcifying cyanobacteria. Front. Microbiol. 9, 1768.

Bontognali, T.R.R., Vasconcelos, C., Warthmann, R.J., Dupraz, C., Bernasconi, S.M., McKenzie, J.A., 2008. Microbes produce nanobacteria-like structures, avoiding cell entombment. Geology 36, 663-666.

Bontognali, T.R.R., McKenzie, J.A., Warthmann, R.J., Vasconcelos, C., 2014. Microbially influenced formation of Mg-calcite and Ca-dolomite in the presence of exopolymeric substances produced by sulphate-reducing bacteria. Terra Nova 26, 72-77.

Cam, N., Georgelin, T., Jaber, M., Lambert, J. F., & Benzerara, K., 2015. In vitro synthesis of amorphous Mg-, Ca-, Sr- and Ba-carbonates: What do we learn about intracellular calcification by cyanobacteria? Geochim. Cosmochim. Acta 161, 36-49.

De Yoreo, J.J., Zepeda-Ruiz, L.A., Friddle, R.W., Qiu, S.R., Wasylenki, L.E., Chernov, A.A., Gilmer, G.H., Dove, P.M., 2009. Rethinking classical crystal growth models through morlcular scale insights: Consequnences of kink-limited kinetics. Cryst. Growth Des. 9(12), 5135-5144.

De Yoreo, J.J., Gilbert, P.U.P.A., Somerdijk, N.A.J.M., Penn, R.L., Whitelam, S., Joester, D., Zhang, H., Rimer, J.D., Navrotsky, A., Banfield, J.F., Wallace, A.F., Michel, F.M., Meldrum, F.C., Cölfen, H., Dove, P.M., 2015. Crystallization by particle attachment in synthetic, biogenic, and geologic environments. Science 349(6247), aaa6760.

Deng, S., Dong, H., Lv, G., Jiang, H., Yu, B., Bishop, M.E., 2010. Microbial dolomite precipitation using sulfate reducing and halophilic bacteria: Results from Qinghai Lake, Tibetan Plateau, NW China. Chem. Geol. 278, 151-159.

Dong, H., Huang, L., Zhao, L., Zeng, Q., Liu, X., Sheng, Y., Shi, L., Wu, G., Jiang, H., Li, F., Zhang, L., Guo, D., Li, G., Hou, W., Chen, H., 2022. A critical review of mineral-microbe interaction and co-evolution: Mechanisms and applications. Nat. Sci. Rev. 9(10), nwac128.

Du, J.S., Bae, Y., De Yoreo, J.J., 2024. Non-classical crystallization in soft and organic materials. Nat. Rev. Mater. 9, 229-248.

Fan, Q., Liu, D., Papineau, D., Qiu, X., Wang, H., She, Z., Zhao, L., 2023. Precipitation of high Mg-calcite and protodolomite using dead biomass of aerobic halophilic bacteria. J. Earth. Sci. 34, 456-466.

Goetschl, K.E., Dietzel, M., Purgstaller, B., Grengg, C., Mavromatis, V., 2021. Control of $MgSO_4^0$(aq) on the transformation of amorphous calcium carbonate to high-Mg calcite and long-term reactivity of the crystalline solid. Geochim. Cosmochim. Acta 312, 357-374.

Gong, Y.U.T., Killian, C.E., Olson, I.C., Appathurai, N.P., Amasino, A.L., Martin, M.C., Holt, L.J., Wilt, F.H., Gilbert, P.U.P.A., 2011. Phase transitions in biogenic amorphous calcium carbonate. Proc. Natl. Acad. Sci. U. S. A. 109(16), 6088-6093.

Gránásy, L., Pusztai, T., Tegze, G., Warren, J.A., Douglas, J.F., 2005. Growth and form of spherulites. Phys. Rev. E 72, 011605.

Gregg, J.M., Bish, D.L., Kaczmarek, S.E., Machel, H.G., 2015. Mineralogy, nucleation and growth of dolomite in the laboratory and sedimentary environment: a review. Sedimentology 62, 1749-1769.

Grünewald, T.A., Checchia, S., Dicko, H., Moullac, G.L., Koua, M.S., Vidal-Dupiol, J., Duboisset, J., Nouet, J., Grauby, O., Michiel, M.D., Chamard, V., 2022. Structure of an amorphous calcium carbonate phase involved in the formation of *Pinctada margaritifera* shells. Proc. Natl. Acad. Sci. U. S. A. 119(45), e2212616119.

Han, Z., Qi, P., Zhao, Y., Guo, N., Yan, H., Tucker, M.E., Li, D., Wang, J., Zhao, H., 2022. High Mg/Ca molar ratios promote protodolomite precipitation induced by the extreme halophilic bacterium *Vibrio harveyi* QPL2. Front. Microbiol. 13, 821968.

Han, Z., Li, J., Zhao, Y., Chen, Q., Gao, X., Hu, K., Guo, N., Wei, X., Meng, R., Zhu, C., Tucjer, M.E., 2024. Dissolved Mn^{2+} promotes microbially-catalyzed protodolomite precipitation in brackish oxidized water. Chem. Geol. 650, 121986.

Ihli, J., Kim, Y.Y., Noel, E.H., Meldrum, F.C., 2013. The effect of additives on amorphous calcium carbonate (ACC): Janus behavior in solution and the solid state. Adv. Funct. Mater. 23(12), 1575-1585.

Jehannin, M., Rao, A., Cölfen, H., 2019. New horizons of nonclassical crystallization. J. Am. Chem. Soc. 141(26), 10120-10136.

Kaczmarek, S.E., Gregg, J.M., Bish, D.L., Machel, H.G., Fouke, B.W., MacNeil, A., Lonnee, J., Wood, R., 2017. Dolomite, very-high magnesium calcite, and microbes: implications for the microbial model of dolomitization. SEPM Spec. Publ. 109, 1-14.

699 Kenward, P.A., Fowle, D.A., Goldstein, R.H., Ueshima, M., González, L.A., Roberts,
700 J.A., 2013. Ordered low-temperature dolomite mediated by carboxyl-group
701 density of microbial cell walls. AAPG Bull. 97, 2113-2125.

702 Kim, J., Kimura, Y., Puchala, B., Yamazaki, T., Becker, U., Sun, W., 2023.
703 Dissolution enables dolomite crystal growth near ambient conditions. Science
704 382, 915-920.

705 Lenders, J.J.M., Dey, A., Bomans, P.H.H., Spielmann, J., Hendrix, M.M.R.M., de
706 With, G., Meldrum, F.C., Harder, S., Sommerdijk, N.A.J.M., 2012.
707 High-magnesian calcite mesocrystals: A coordination chemistry approch. J.
708 Am. Chem. Soc. 134, 1367-1373.

709 Littlewood, J.L., Shaw, S., Peacock, C.L., Bots, P., Trivedi, D., Burker, I.T., 2017.
710 Mechanism of enhanced strontium uptake into calcite via an amorphous
711 calcium carbonate crystallization pathway. Cryst. Growth Des. 17(3),
712 1214-1223.

713 Liu, D., Yu, N., Papineau, D., Fan, Q., Wang, H., Qiu, X., She, Z., Luo, G., 2019a.
714 The catalytic role of planktonic aerobic heterotrophic bacteria in
715 protodolomite formation: Results from Lake Jibuhulangtu Nuur, Inner
716 Mogolia, China. Geochim. Cosmochim. Acta 263, 31-49.

717 Liu, D., Xu, Y., Papineau, D., Yu, N., Fan, Q., Qiu, X., Wang, H., 2019b.
718 Experimental evidence for abiotic formation of low-temperature
719 proto-dolomite facilitated by clay minerals. Geochim. Cosmochim. Acta 247,
720 83-95.

721 Liu, D., Fan, Q., Papineau, D., Yu, N., Chu, Y., Wang, H., Qiu, X., Wang, X., 2020a.
722 Precipitation of protodolomite facilitated by sulfate-reducing bacteria: The
723 role of capsule extracellular polymeric substances. Chem. Geol. 533, 119415.

724 Liu, D., Xu, Y., Yu, Q., Yu, N., Qiu, X., Wang, H., Papineau, D., 2020b. Catalytic
725 effect of microbially-derived carboxylic acids on the precipitation of
726 Mg-calcite and disorderd dolomite: Implications for sedimentary dolomite
727 formation. J. Asian Earth Sci. 193, 104301.

728 Lotsari, A., Rajasekharan, A.K., Havarsson, M., Andersson, M., 2018.
729 Transformation of amorphous calcium phosphate to bone-like apatite. Nat.
730 Commun. 9, 4170.

731 McKenzie, J.A., Vasconcelos, C., 2009. Dolomite Mountains and the origin of the
732 dolomite rock of which they mainly consist: historical developments and new
733 perspectives. Sedimentology 56, 205-219.

734 Mehta, N., Vantelon, D., Gaëtan, J., Fernandez-Martinez, A., Delbes, L., Travert, C.,
735 Benzerara, K., 2023. Calcium speciation and coordination envrionment in
736 intracellular amorphous calcium carbonate (ACC) formed by cyanobacteria.
737 Chem. Geol. 641, 121765.

738 Mergelsberg, S.T., De Yoreo, J.J., Miller, Q.R.S., Michel, F.M., Ulrich, R.N., Dove,
739 P.M., 2020. Metastable solubility and local structure of amorphous calcium
740 carbonate. Geochim. Cosmochim. Acta 289, 196-206.

741 Monteil, C.L., Benzerara, K., Menguy, N., Bidaud, C.C., Michot-Achdjian, E.,
742 Bolzoni, R., Mathon, F.P., Coutaud, M., Alonso, B., Garau, C., Jézéquel, D.,
743 Viollier, E., Ginet, N., Floriani, M., Swaraj, S., Sachse, M., Busigny, V.,
744 Duprat, E., Guyot, F., Lefevre, C.T., 2020. Intracellular amorphous
745 Ca-carbonate and magnetite biomineralization by a magnetotactic bacterium
746 affiliated to the Alphaproteobacteria. ISME J. 15, 1-18.

747 Mullin, J.W., 2001. Crystallization, 4th ed., Butterworth Heinemann, Boston.
748 Nyirö-Kósa, I., Rostási, A., Bereczk-Tompa, É, Cora, I., Koblar, M., Kovács, A.,
749 Pósfai., 2018. Nucleation and growth of Mg-bearing calcite in a shallow,
750 calcareous lake. Earth Planet. Sci. Lett. 496, 20-28.

751 Perri, E., Tucker, M., 2007. Bacterial fossils and microbial dolomite in Triassic
752 stromatolites. Geology 35(3), 207-210.

753 Petrash, D.A., Bialik, O.M., Bontognali, T.R.R., Vasconcelos, C., Roberts, J.A.,
754 McKenzie, J.A., Konhauser, K.O., 2017. Microbially catalyzed dolomite
755 formation: From near-surface to burial. Earth-Sci. Rev. 171, 558-582.

756 Purgstaller, B., Mavromatis, V., Immenhauser, A., Dietzel, M., 2016. Transformation
757 of Mg-bearing amorphous calcium carbonate to Mg-calcite: In situ
758 monitoring. Geochim. Cosmochim. Acta 174, 180-195.

759 Purgstaller, B., Mavromatis, V., Goetschl, K.E., Steindl, F.R., Dietzel, M., 2021.
760 Effect of temperature on the transformation of amorphous calcium magnesium
761 carbonate with near-dolomite stoichiometry into high Mg-calcite.
762 CrystEngComm 23, 1969-1981.

763 Qiu, X., Wang, H., Yao, Y., Duan, Y., 2017. High salinity facilitates dolomite
764 precipitation mediated by *Haloferax volcanii* DS52. Earth Planet. Sci. Lett.
765 472, 197-205.

766 Radha, A.V., Fernandez-Martinez, A., Hu, Y., Jun, Y.S., Waychunas, G.A.,
767 Navrotsky, A., 2012. Energetic and structural studies of amorphous
768 $Ca_{1-x}Mg_xCO_3 \cdot nH_2O$ ($0 \leq x \leq 1$). Geochim. Cosmochim. Acta 90, 83-95.

769 Raudsepp, M.J., Wilson, S.A., Morgan, B., Patel, A., Johnston, S.G., Ganem, E.J.,
770 Fallon, S.J., 2022. Non-classical crystallization of very high magnesium
771 calcite and magnesite in the Coorong Lakes, Australia. Sedimentology 69(5),
772 2246-2266.

773 Roberts, J.A., Bennett, P.C., González, L.A., Macpherson, G., Milliken, K.L., 2004.
774 Microbial precipitation of dolomite in methanogenic groundwater. Geology
775 32, 277-280.

776 Roberts, J.A., Kenward, P.A., Fowle, D.A., Goldstein, R.H., González, L.A., Moore,
777 D.S., 2013. Surface chemistry allows for abiotic precipitation of dolomite at
778 low temperature. Proc. Natl. Acad. Sci. U. S. A. 110, 14540-14545.

779 Rodriguez-Blanco, J.D., Shaw, S., Benning, L.G., 2011. The kinetics and mechanisms
780 of amorphous caclcium carbonate (ACC) crystallization to calcite, via vaterite.
781 Nanoscale 3, 265-271.

782 Rodriguez-Blanco, J.D., Shaw, S., Benning, L.G., 2015. A route for the direct
783 crystallization of dolomite. Am. Mineral. 100, 1172-1181.

784 Sánchez-Román, M., Vasconcelos, C., Schmid, T., Dittrich, M., McKenzie, J.A.,
785 Zenobi, R., Rivadeneyra, M.A., 2008. Aerobic microbial dolomite at the
786 nanometer scale: Implications for the geologic record. Geology 36, 879-882.

787 Sugawara, S., Fujiya, W., Kagi, H., Yamaguchi, A., Hashizume, K., 2022.
788 Heat-induced dolomitization of amorphous calcium magnesium carbonate in a
789 CO_2-filled closed system. ACS Omega 7(49), 44670-44676.

790 Sun, F., Hu, W., Wang, X., Hu, Z., Wu, H., Guo, Y., Wei, G., 2023.
791 Methanogen-mediated dolomite precipitation in an early Permian lake in
792 northwestern China. GSA Bull. https://doi.org/10.1130/B37156.1

793 van der Mei, H.C., Bos, R., Busscher, H.J., 1998. A reference guide to microbial cell
794 surface hydrophobicity based on contact angels. Colloid. Surface. B 11(4),
795 213-221.

796 Vasconcelos, C., McKenzie, J.A., Bernasconi, S., Grujic, D., Tiens, A.J., 1995.
797 Microbial mediation as a possible mechanism for natural dolomite formation
798 at low temperatures. Nature 377, 220-222.

799 Wang, D., Wallace, A. F., De Yoreo, J. J., Dove, P. M., 2009. Carboxylated
800 molecules regulate magnesium content of amorphous calcium carbonates
801 during calcification. Proc. Natl. Acad. Sci. U. S. A. 106, 21511-21516.

802 Warren, J., 2000. Dolomite: occurrence, evolution and economically important
803 associations. Earth-Sci. Rev. 52, 1-81.

804 Xu, J., Yan, C., Zhang, F., Konishi, H., Xu, H., Teng, H.H., 2013. Testing the
805 cation-hydration effect on the crystallization of Ca-Mg-CO_3 systems. Proc.
806 Natl. Acad. Sci. U. S. A. 110, 17750-17755.

807 Yu, P.T., Tsao, C., Wang, C.C., Chang, C.Y., Wang, C.H., Chan, J.C.C., 2017.
808 High-magnesium calcite mesocrystals: Formation in aqueous solution under
809 ambient conditions. Angew. Chem. Int. Ed. 56, 16202-16206.

810 Zhang, F., Xu, H., Konishi, H., Kemp, J.M., Roden, E.E., Shen, Z., 2012. Dissolved
811 sulfide-catalyzed precipitation of disordered dolomite: Implications for the

formtion mechanism of sedimentary dolomite. Geochim. Cosmochim. Acta 97, 148-165.

Zhang, F., Xu, H., Shelobolina, E.S., Konishi, H., Converse, B., Shen, Z., Roden, E.E., 2015. The catalytic effect of bound extracellular polymeric substances excreted by anaerobic microorganisms on Ca-Mg carbonate precipitation: Implications for the “dolomite problem”. Am. Mineral. 100, 483-494.

Zhang, F., Xu, H., Shelobolina, E.S., Konishi, H., Roden, E.E., 2021. Precipitation of low-temperature disordered dolomite induced by extracellular polymeric substances of methanogenic archaea *Methanosarcina barkeri*: Implications for sedimentary dolomite formation. Am. Mineral. 106, 69-81.

Zheng, W., Liu, D., Yang, S., Fan, Q., Papineau, D., Wang, H., Qiu, X., Chang, B., She, Z., 2021. Transformation of protodolomite to dolomite proceeds under dry-heating conditions. Earth Planet. Sci. Lett. 576, 117249.